Infrared Free Induction Decay (IR-FID) of Non-Interfacial Origin Observed in the Interfacial Sum-Frequency Generation Vibrational Spectroscopy (SFG-VS)

Bo-Jun Zhao[1,2], Xing-Xing Peng[2,3], Li Zhang[1,2], Jing-Ming Cao[1,2], Shu-Yi Yang[1,2], An-An Liu[2,3], and Hong-Fei Wang[2,3*]

[1]*Department of Chemistry, Zhejiang University, Yuhangtang Road, Westlake District, Hangzhou, Zhejiang Province, 310058*

[2]*School of Science, Westlake University, No. 600 Dunyu Road, Sandun Town, Westlake District, Hangzhou, Zhejiang Province, 310030*

[3]*Institute of Natural Sciences, Westlake Institute for Advanced Study, Hangzhou, Zhejiang Province, 310024, China*

Corresponding Author

*(H.-F. Wang) E-mail: wanghongfei@westlake.edu.cn

ORCID

Bo-Jun Zhao: 0000-0002-2926-4371

Xing-Xing Peng: 0000-0003-1468-2770

Li Zhang: 0000-0002-2905-8260

Shu-Yi Yang: 0009-0000-9138-4609

An-An Liu: 0009-0001-8191-6111

Hong-Fei Wang: 0000-0001-8238-1641

ABSTRACT

We report the observation of infrared free induction decay (IR-FID) signal of the anti-symmetric modes around ~ 2350 cm^{-1} of the gaseous CO_2 molecules in the air in the sum-frequency generation vibrational spectroscopy (SFG-VS) measurement from the gold surface. These signals appeared with time-dependent interference pattern in the 15-73 ps range and beyond after the time-zero of the SFG-VS process. The interference pattern was found to reflect the rotational coherence of the gaseous CO_2 molecules. Similar IR-FID and rotational coherence was also observed for the symmetric and asymmetric stretching modes of gaseous H_2O molecules in air. The gold surface in this case serves as the up-conversion agent with the visible pulse as the time-gate for the ultrafast IR-FID emissions. We tested this hypothesis by replacing the gold surface with a β-BBO (beta-barium borate, β-BaB_2O_4) and found a five orders of magnitude increase of the signal in the reflecting geometry. The up-conversion of the IR-FID radiation of non-interfacial origin into the SFG-VS signal also provides the mechanistic understanding of the 'abnormal spectral bands' in broadband SFG-VS induced by bulk absorption and refraction reported in the literature.

Key Words: Infrared Free Induction Decay; Sum-Frequency Generation; Time-Resolved; Carbon Dioxide; Rotational Coherence; Up-Conversion;

TABLE OF CONTENTS (TOC) GRAPHICS

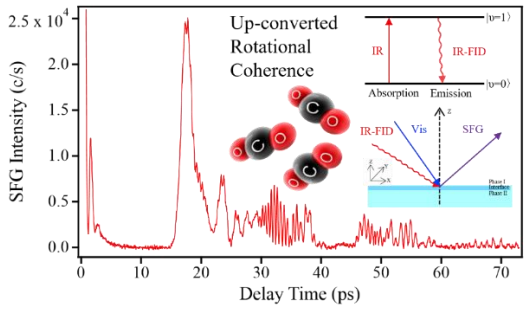

I. INTRODUCTION

Here, we report the unexpected observation of the infrared free induction decay (IR-FID) signal of gaseous molecules or thin film materials in the ultrafast IR beam path, up-converted at the gold surface, in the frequency and time-resolved surface sum-frequency generation vibrational spectroscopy (SFG-VS) measurement.

Free induction decay (FID) is the coherent radiation from the induced polarization of the molecular or atomic system after the interaction with an short pump pulse, as long as the duration of the pulse is shorter than the dephasing time of the system. Nuclear FID was proposed and observed in nuclear magnetic resonance (NMR) in the late 1940s.[1,2] The NMR FID processes usually happens in the ~100 microsecond time scale. The optical FID in the visible region were observed at the microsecond time-scales in the early 1970s.[3,4] Optical FID (OFID) has been observed in gases,[3, 5] molecular beams,[6, 7]and solids [6, 8-10]. With the development of ultrafast lasers, IR-FID of liquids were studied in the early 1990s at sub-picosecond time-resolution using either transient absorption IR spectroscopy[11, 12] or visible pulse up-conversion of the IR radiation.[13] In recent years, there are also sub-picosecond and picosecond IR-FID,[14, 15] as well as ultrafast Terahertz (THz)-FID, studies on gaseous molecules.[16]

SFG-VS is the coherent second-order nonlinear spectroscopy with sub-monolayer sensitivity and interfacial selectivity, widely used for quantitatively characterization of molecular orientation and conformation, interaction, and dynamics of surfaces and at interfaces, with applications in chemistry, energy, materials, environment and biological sciences.[17-19] In a normal SFG-VS experiment, a visible light (ω_1) and an infrared (IR) light (ω_2) are overlapped spatially and temporally at the interface to produce a sum frequency signal ($\omega_1 + \omega_2$).[19] When the IR light frequency resonates with the molecular vibrational transitions, or the visible light frequency resonates with the molecular electronic transitions, the SFG-VS get vibrationally or electronically enhanced to obtain the spectra of the interfacial molecular species. The interfacial selectivity of SFG-VS comes from the symmetry requirement which dictates that the SFG-VS process is forbidden for the centrosymmetric media (molecular system) under the dipole approximation.

Therefore, as the interface is intrinsically without centrosymmetry, SFG-VS is allowed for interface. With the advancement in laser technology and photo-detection technology, SFG-VS spectra from molecules with sub-monolayer surface density is readily detectable, making SFG-VS a uniquely powerful spectroscopic technique for interfacial studies. [17-22]

SFG-VS FID was first reported by Guyot-Sionnest et. al. in 1991 on the vibrational dynamics of the Si−H bond on a silicon (111) surface in the 10s of picosecond.[23] In a SFG-FID experiment, a short IR pulse coherently excites vibrational oscillators to create a coherent vibrational wave-packet. As the coherent vibrational polarization decays with time due to the loss of coherence, a short visible pulse probes the remaining coherence by generating a sum frequency polarization. Time-scanning the visible pulse against the initial IR pulse generates a SFG-VS signal in the time-domain, obtaining the time evolution of the vibrational polarization through the so-called SFG-FID process. So far, there have been SFG-FID studies on the dephasing dynamics of many different interfacial vibrations, such as, -CO stretching vibrations at vacuum/Cu(111) interface[24], -CH_2 and -CH_3 vibrations of a ferric stearate [$Fe(CH_3(CH_2)_{16}CO_2)_3$] monolayer at air/$CaF_2$ interface[25], -CH and -CN stretch vibrations at Au/CH_3CN liquid interface[26], -OD stretch at D_2O/CaF_2 interface[27], -CH_2 and -CH_3 vibrations of heptadecanoic acid (HDA) Langmuir-Blodgett monolayer at air/quartz interface,[28] -C≡C- stretch of propiolic acid (PA) at air/water interface,[29] -CH_2 and -CH_3 vibrations of octadecyltrichlorosilane (OTS) on fused silica surface,[30] -CH_3 stretch of methyl-terminated Si(111) surface,[31] interface, -CN stretch of 4-n-octyl-4'-cyanobiphenyl (8CB) Langmuir monolayer at air/water interface[32], -CH stretching vibrations at air/DMSO (dimethyl sulfoxide) interface[33], free -OH stretch oscillators at charged (pH ≈ 13, KOH) interface of alumina/water (Al_2O_3/H_2O)[34].

Unlike the FID process in NMR or IR-FID, in the SFG-FID, the visible probe pulse directly interacts with the probed molecules at the interface undergone vibrational dephasing processes after the initial coherence excitation; while the emitted FID signal in the NMR was detected directly by the detector, or in the IR-FID the emitted IR signal is upconverted with a time-gating short visible pulse before it is detected. Therefore, the SFG-FID signal is subjected to the symmetry

and polarization selection rules of the second order SFG-VS processes, i.e., both IR and visible polarizations, and the symmetries of the vibrational and electronic states count; while the NMR or IR-FID signal is only subject to the first order NMR or IR absorption and emission process.

Even though the SFG-FID and the visible pulse upconverted IR-FID signal from the same molecule are in the same spectral range, as long as the same visible pulse frequency is employed, or even with similar or overlapping time-scale for their vibrational coherence, there has been no report for the detection of both the SFG-FID and the IR-FID in the same experiment, or to be specific, no observation of IR-FID process in the SFG-FID measurement. This is not hard to understand because SFG-FID is an interface process, while the IR-FID is usually a bulk process. The two processes simply do not go together in the same experiment, as one usually believes.

In this report, we present the unexpected observation of IR-FID signal of the anti-symmetric modes around ~2350 cm^{-1} of the gaseous CO_2 molecules in the air in the SFG-VS measurement from a gold surface. The time dependent signal also showed oscillation patterns corresponding to the rotational coherence belong to the CO_2 molecules. It turned out that the gold surface served as the up-conversion medium for the IR-FID signal emitted from the gaseous CO_2 molecules in the ultrafast IR beam path, by the 800nm visible light used to generate SFG-VS signal from the gold surface. Replacing the gold surface with a β-BBO (beta-barium borate, β-BaB_2O_4) crystal can increase the up-converted signal by 10^5 fold. Changing the broad ultrafast IR pulse from the 2350 cm^{-1} band to the 3700 cm^{-1} also enabled us to observe the IR-FID signal emitted from the symmetric and anti-symmetric stretching vibrational modes of the atmospheric H_2O molecules in the IR beam pass. The IR-FID signal also showed rotational coherence patterns for the gaseous H_2O molecules. This discovery of the up-converted IR-FID radiation signal of the gaseous molecules, as well as of a thin polyethylene (PE) film in the IR beam path, in the SFG-VS measurement also provides a mechanistic understanding of the 'abnormal spectral bands' in broadband SFG-VS induced by bulk absorption and refraction reported in the literature.[35, 36]

II. EXPERIMENTALS

The SFG-VS setup (Figure 1) in this work is based on a 7 W Ti:Sapphire laser amplifier system (1kHz, Astrella, Coherent) with a typical 35 fs pulse width and a center wavelength of 800 nm. In order to perform time-resolved SFG-FID[32] and frequency resolved broadband SFG-VS (BB-SFG-VS) [20, 37, 38] measurements in this work, broadband mid-IR pulses, sub-100fs femtosecond 800 nm pulses, and ~2ps 800nm pulses needs to be generated.

The details of the experimental setup and conditions are below.

Broadband IR Unit. About 2.7 mJ output of the 800 nm light from the femtosecond regenerative amplifier is used to pump a collinear optical parametric amplifier (OPA, TOPAS-Prime, Light Conversion). The OPA outputs a signal pulse in the range of 1.1~1.6 um and an idler pulse in the range of 1.6~2.6 um. The signal and idler beams are collinear and they are directly sent into a silver gallium disulfide crystal ($AgGaS_2$, 8*8*0.4 mm, θ = 39º, ϕ = 45º, Chengdu DIEN TECH, Co., Ltd.), to generate a tunable fs broad-band mid-IR in the range of 2.6-12 um through a different frequency generation (DFG) process. Change of the center frequency of the output broadband mid-IR band is controlled by computer tuning of the frequency of the signal and idler pair from the TOPAS output, and the energy and band profile is fine-tuned by rotating the $AgGaS_2$ angle. The IR spectral profile is monitored with the SFG-VS signal on a gold film surface using a picosecond 800 nm pulse. Typically, the 3.95 um (2530 cm^{-1}) band used in the CO_2 measurement has a full width at half-maximum (FWHM) of 340 cm^{-1} (Figure 2A) with an unpurged energy of about 45 μJ after the long pass mid-IR filter (Filter 1 in Figure 1, coated CVD-ZnSe window, ϕ25.4*3 mm, high transmission 3-12 μm, Light Conversion) behind the DFG crystal. After the delivering optics, this IR power is typically about 25 μJ/pulse at the sample surface position. The 2.70 um (3700 cm^{-1}) band used in the H_2O measurement has a FWHM of 380 cm^{-1} with an unpurged energy of about 22 μJ after the Filter 1. The 3.45 um (2900 cm^{-1}) band used in the C-H stretching region measurement has a FWHM of 350 cm^{-1} with an unpurged energy of about 50 μJ after the Filter 1.

Picosecond (ps) Visible Unit. A ~1.2 mJ output of the femtosecond regenerative amplifier pass through a zero-chirp 4f (4* focal length *f*) pulse shaper[27, 38-42] to produce a spectrally narrowed

picosecond visible beam with a 10 cm^{-1} FWHM at about 2.4 ps time width, the pulse energy near the sample surface is about ~20 μJ per pulse. The 4f pulse shaper system consists of a transmissive grating (TG) optimized at 800 nm (990 l/mm, 805 nm, Wasatch Photonics), a planoconvex cylindrical lens (CL) (f=200 mm), an adjustable width slit (M-SV-0.5, Newport), and a 0° reflection dielectric mirror (HR@750-850 nm, ϕ 25.4 mm, AOI=0°, Low GDD, CRYSTOCK). The slit width is tunable to control the bandwidth of the visible beam as well as the pulse duration. The output power is inversely proportional to the slit width, and the position of the slit determines the center wavelength as well as the power of the outgoing laser pulse within the bandwidth of the 800nm femtosecond input pulse. The 10 cm^{-1} FWHM and 2.4 ps time width pulse was generated with a slit width about 200 μm positioned near the center of the dispersed 800nm band.

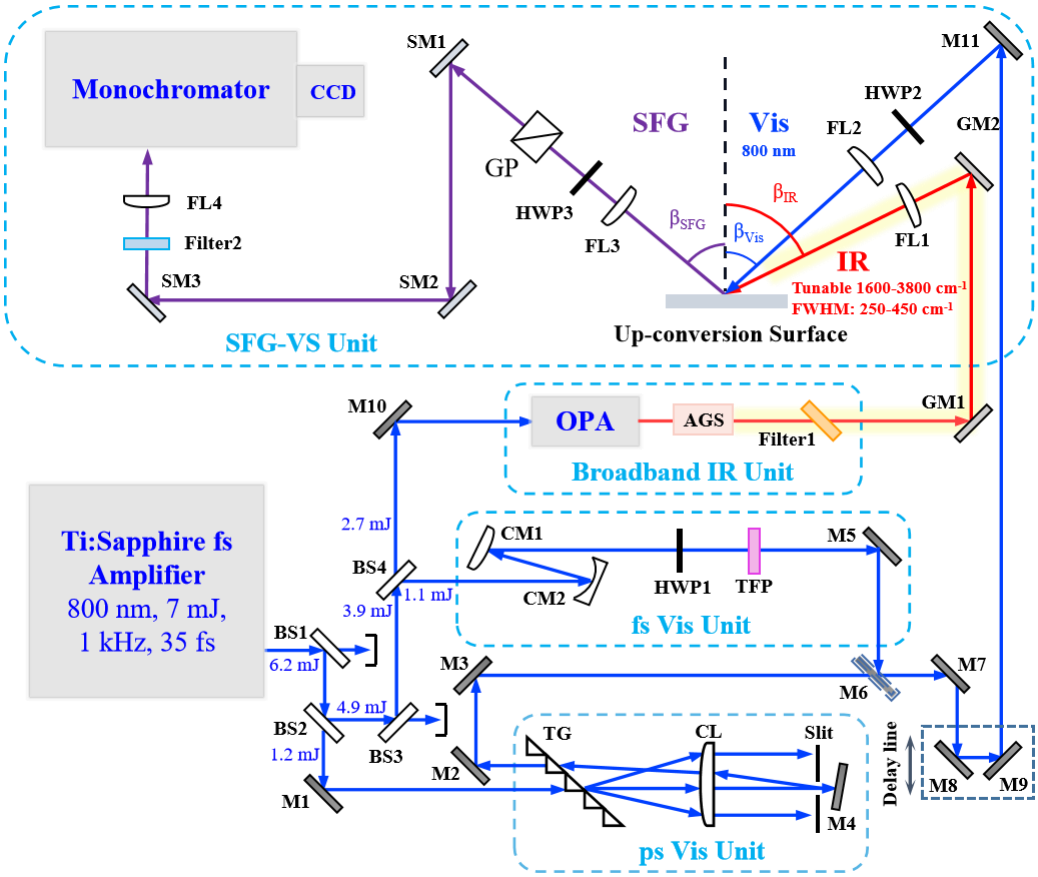

FIG. 1. A schematic of the experimental setup for BB-SFG-VS and up-converted infrared FID on surface. M6 (a dielectric high reflection mirror with a magnetic base) is used to switch between the fs and ps visible pulses used in the measurement. Notations: BS1-BS4, costed beam splitters; M1-M11, high-reflection dielectric mirror for 800 nm; GM1-GM2, gold mirror for broadband IR; SM1-SM3, sliver mirror for SFG signal; TG, transmission grating; CL, plano-convex cylindrical lens; CM1, concave mirror; CM2, convex

mirror; HWP1-HFW3, half-wave plate; TFP, thin film polarizer; OPA, optical parametric amplifier; AGS, $AgGaS_2$ crystal for difference frequency generation; Filter1, long pass mid-IR filter transmitting 3-12um fs broadband IR pulse, reflecting signal pulse (1.1~1.6 um) and idler pulse (1.6~2.6 um); Filter2, 780 nm short pass filter; GP, Glan Prism; FL1-FL4, focusing lens. The light-yellow area represents the optical path under purging, which ends about 25mm before the sample surface.

Femtosecond (fs) Visible Unit. A ~1 mJ 35 fs 800 nm visible pulse is beam size-reduced by half and collimated with a reflecting telescope consists of a concave mirror (f = 500 mm) and a convex mirror (f = 250 mm). A half-wave plate (1/2 WP, @650-1100 nm, WPA2415, Union Optics) and a thin film polarizer (TFP, @780-820 nm, G118101TFP-1-1, Bc-light) are used to tune the power of the 800nm beam. Most of the time, the pulse energy is tuned to <10 μJ at the gold sample surface to avoid supercontinuum generation. With a dielectric mirror on a movable magnet base (M6), the fs visible beam and the ps visible beam can share the optical path after the mirror M7.

IR Purging System. Aluminum tube is used to cover most part of the IR optical beam path between the DFG crystal and the sample stage, to reduce the IR absorption due to atmospheric CO_2 and H_2O vapors. Nitrogen gas from the vaporized liquid nitrogen tank slowly flow through the aluminum tube to purge the CO_2 and H_2O vapors in the tube. With the purging gas on the IR-FID signal would disappear from the SFG-VS signal from the gold surface.

SFG-VS Unit. The time delay between the IR and visible (both fs and ps beams) are controlled with a motorized delay stage (2μm/step, FMS80-100, Feinixs Inc.) in the visible beam path with M8 and M9 mirrors.

The broadband IR beam is focused on to the sample surface with a plano-convex lens with 200 mm focal length. The focal point is slightly above the surface to control the power density on the sample surface to avoid damaging of the sample surface. The typical spot size on the sample surface is about ~300 μm in diameter. The fs or the ps visible beam is focused onto the sample surface with a 315 mm focal length plano-convex lens. Similar to the IR beam, the focal point is slightly above the sample surface, and the typical spot size on the sample surface is about ~500

μm in diameter. The polarization of the visible beam is tuned with a half-wave plate (HWP2, @650-1100 nm, WPA2415, Union Optics). The incident angles of visible and IR beam in this experiment are 47º ± 1º, and 65º ± 1º with respect to the surface normal, respectively, making the SFG-VS signal outgoing angle as 49º ± 1º in the reflecting geometry.

SFG-VS Detection Unit. The SFG-VS signal is collected and collimated by a focal lens (FL3, focal length = 150 mm). The halfwave plate (HWP3, @450-650 nm) and a Glan-Taylor prism polarizer (GP, @350-2300 nm, PGL5012EW, Union Optics) forms a polarization unit. The GP is fixed at the *p* polarization (polarization within the vertical optical incident plane), and the HWP3 rotates the polarization of the SFG-VS signal in different polarizations to ensure the detector always receive them in the same *p* polarization. The SFG-VS signal is delivered to the spectrometer (Acton SP-2500, 1200 l/mm, Princeton Instruments) and a thermoelectric cooled CCD (ProEM 1600*200 pixels, 16 μm/pixel, Princeton Instruments) detector guided with three silver mirrors (SM1-3, HR 0.4-12 μm, Union Optics) and through a short pass filter (Filter 2, short pass 780 nm) and a matching focal lens (FL4, f = 40 mm). In some cases, additional short pass filters or notch filters, or even dark covers before the spectrometer, need to be added to effectively block the scattering 800 nm lights in the room.

Samples and Data Collection. Several substrate surfaces are used in this work. Gold film plate (AOI = 0º, 98% HR 2-12 mm, 100 nm gold film with a 100 nm SiO_2 protection film on 6.35 mm K9 glass, Union Optics) is used for broadband SFG-VS reference surface, as in many other broadband SFG-VS works. In measuring the small SFG-VS signal on glass surface, a round K9 glass plate (ϕ25 mm x 2 mm) with half of its area coated with gold film is used. The gold film (~ 500 nm thick) is coated through an Electron Beam Evaporation coating system. Thick right-handed z-cut α-quartz (12.5*12.5*10 mm, Sinoma Synthetic Crystals Co., Ltd. is also used for SFG-VS signal reference, usually with the α-quartz azimuthal angle set at φ = 90º. After we found that gold surface can be used for up-conversion of the IR-FID signal in the SFG-VS experimental geometry,

a beta-barium borate (β-BBO, β-BaB_2O_4, 7*7*1 mm, CRYSTOCK) crystal is used as the up-conversion medium to amplify the IR-FID in the reflecting geometry.

The polyethylene (PE) film (PE, art. NO. 306001, Chahua Modern Housewares Co. Ltd.) is with a thickness of 10 μm as used in literature.[35]

Broadband SFG-VS signal can be measured in both frequency domain and time-domain. In the frequency-domain experiment, picosecond visible and femtosecond IR were used. Typically, the signal in the ppp polarization combination was taken with a 30 second exposure, the spectra were usually averaged three times. The integrated intensity signal for the IR-FID or the SFG-FID was measured in the time-domain, with the fs visible pulses delayed 30 fs per step against the IR pulses.[27, 32, 33, 43] The integrated spectral intensity at each data point was averaged three times with 1 second exposure each for CO_2, and with 8 second exposure for H_2O, which has smaller signal than that of CO_2.

Experimental Condition. All experiments were carried out in a Class 1000 clean room with a controlled temperature of 21.0 ± 0.2 °C, and at ambient pressure, and the relative humidity is < 40%. The particle counts on the optical table is about Class 100 (FED-STD-209 E).

III. RESULTS AND DISCUSSION

1. The Unexpected Time-Dependent SFG-VS Signal from the Gold Film Surface

One of the surprising observations when making time-dependent broadband SFG-VS measurement using <100 fs visible pulse on neat gold surface in the 2200-2800 cm^{-1} region (Figure 2 A-B) was that there was observable broadband signal in the range of 2300-2380 cm^{-1} when the femtosecond visible pulse was delayed more than 15 picosecond against the broadband femtosecond IR pulse. Using ~2.4 ps visible pulse (Figure C-D), one can observe those time dependent spectra much clearly with a spectral resolution about 10 cm^{-1} (Figure 3). However, those signal in Figure 3 completely disappeared after ~200 fs delay (Figure 4B) when the optical path of the femtosecond IR pulse was purged with N_2 gas. Purge or no-purge, the gold film surface is

always exposed in the ambient air. Therefore, the observed time-dependent signal is originated from the un-purged IR beam path, instead of anything on the gold film surface. Since the IR absorption of the atmospheric CO_2 antisymmetric vibrational stretching modes is in this spectral range (Figure 2E), and the absorption is removed when the optical path is purged, the origin of those time-delayed signal in Figure 3 and Figure 4 A-B must have come from the atmospheric CO_2 molecules in the IR optical path. Such phenomenon is unexpected and has not been reported before in the SFG-VS literature.

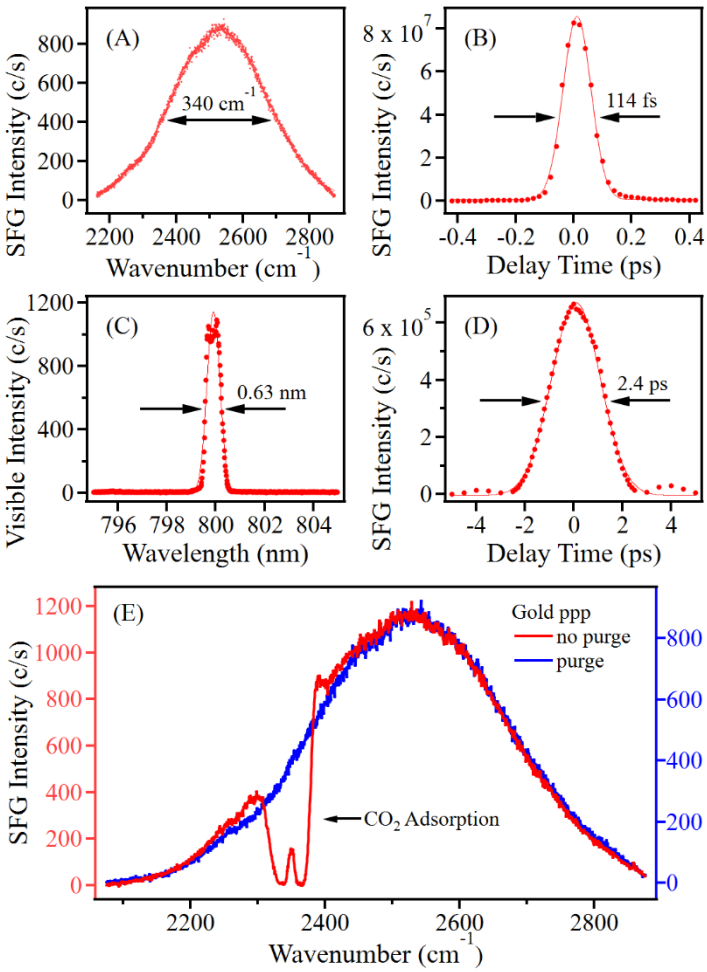

FIG. 2. Characterization of the temporal and frequency profiles of the femtosecond IR pulse (A & B & E) and the picosecond 800nm pulse (C & D). (A) SFG-VS signal on the gold film surface. The spectral full width at half maximum (FWHM) is ~340 cm^{-1}, and the peak center is about 2530 cm^{-1}. (B) The temporal cross-correlation (fs IR and fs Vis) profile of fs Vis pulse used for the FID measurements. The pulse FWHM is about 115 fs, the fs visible pulse is ~80 fs. (C) Spectrum of the narrow-band visible picosecond (ps) pulse.

The spectral FWHM is 0.63 nm (~10 cm^{-1}), central wavenumber is at 800 nm. (D) The temporal cross-correlation (fs IR and ps Vis) profile of ps Vis pulse stretchered by the 4f pulse shaper and used for the BB-SFG measurements. The ps visible pulse FWHM is 2.37 ps. The solid red lines are the results fitted by Gaussian Amp formula to the experimental data (black dots). (E) The BB-SFG-VS at delay=0. The red line shows the BB-SFG-VS absorption spectrum (ro-vibrational spectrum) of the atmospheric CO_2 molecules. The 2349 cm^{-1} peak is assigned to the antisymmetric stretching vibrational mode. Excluding the absorption part, these two lineshapes are overlapped.

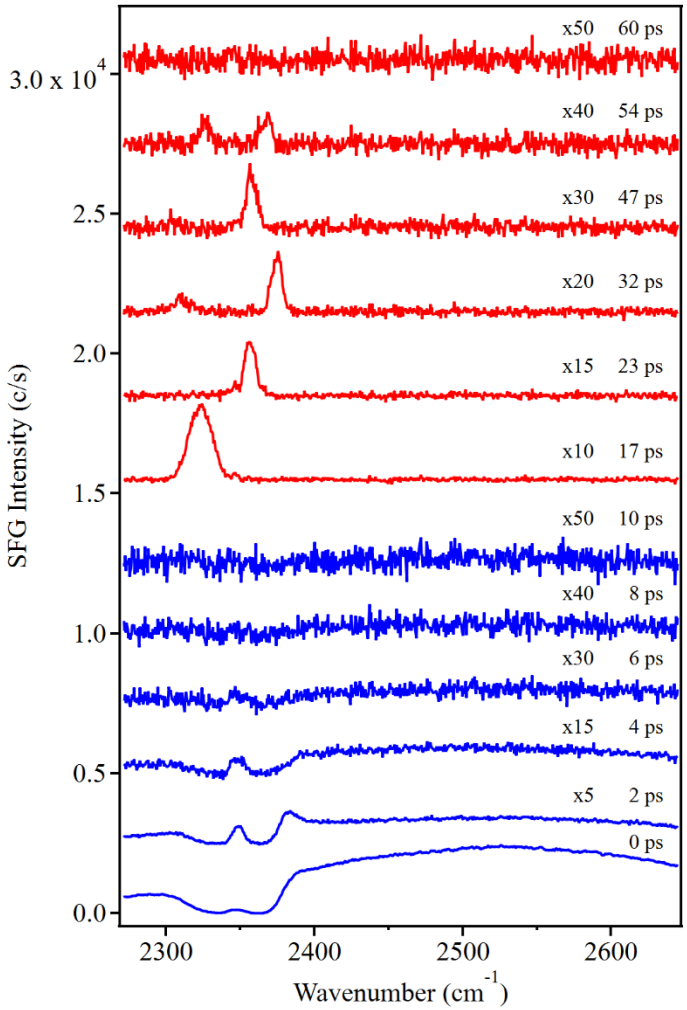

FIG. 3. BB-SFG spectra of the CO_2 molecules on air/gold interface (PPP polarization combination) with different delay time of the picosecond visible pulse (FWHM 2.4ps). The vibrational peaks appeared in the range of 2300-2380 cm^{-1}. Data with different delay times are offset vertically for visual effects. In the 0-10 ps range, it is with a 2500 c/s offset for the next curve (blue line), and in the 10-60 ps range, it is 3000 c/s (red line), respectively.

In order to understand of the nature of the unexpected time-dependent SFG-VS signal, SFG-

VS measurements under different conditions were tested, as in Figure 4.

Figure 4A shows a complete time scan of the SFG-VS signal from the gold film surface from 0 to 73 ps delay of the fs visible pulse against the IR pulse. The spike at the 0 time has a FWHM of ~115 fs is the cross-correlation of the fs visible and IR pulses, indicating that neither of them is broader than ~115 fs, or ~80 fs if they have similar pulse width (Figure 2B). The intensity of the 0 time spike is more than two orders of magnitude stronger than that of the signal in the complicated coherent oscillation pattern in the ~15-70 ps range, and of the sharp peak at ~49 ps with a FWHM of ~130 fs. The time dependent SFG-VS signal in the ~15-73 ps range in Figure 4A also corresponds to the emergence of the time-dependent spectral peaks in the 2300-2380 cm^{-1} range measured with the 2.4 ps visible pulse in Figure 3. Therefore, the oscillation patterns in the time-dependent SFG-VS dynamics is connected to the oscillation of the peak positions with time in the spectra. This connection will be discussed later.

In Figure 4B, the oscillation pattern completely disappears when the IR optical path is purged with N_2 gas. However, the sharp peak at ~ 49 ps remains unchanged. In Figure 4C, both the oscillation pattern and the ~ 49 ps peak completely disappear when the fs visible or IR beam is blocked. Above facts clearly indicate that both the oscillation pattern and the ~49 ps peak are SFG-VS signal in nature, which needs the presence of both the fs visible and IR pulses; while the oscillation pattern is clearly related to the gaseous absorption that is purged in the IR beam path, the ~ 49 ps peak is clearly not thus related. Since the gaseous N_2 has no IR absorption, and the ~ 49 ps peak is with the FWHM close to the pulse width of the cross correlation of the fs visible and IR pulses, its origin has to be related to the side pulse in one of the laser beam which is ~ 49 ps delayed from the main pulse and more than two orders of magnitude weaker. Therefore, any signal induced by this ~ 49 ps band is going to be a few orders smaller than this ~ 49 ps peak in the data, and negligible in our measurement. Nevertheless, the fact that such a weak ~ 49 ps signal can be clearly measured indicates excellent sensitivity, dynamic range and signal-noise-ratio (SNR) in the time-dependent SFG-VS measurement.

The data in Figure 4D further demonstrate that the observed time-dependent SFG-VS is not

related to the molecules on the substrate surface, but the SFG-VS susceptibility of the substrate surface is crucial. The time-dependent SFG-VS oscillation pattern and the ~ 49 ps peak is essentially the same when the SFG-VS is measured from the gold film surface and the thick z-cut α-quartz crystal surface, with smaller intensity of the latter. The signal strength is proportional to the non-resonant SFG-VS signal from these two substrate surfaces in the respective polarizations. In comparison, there is no such time-dependent SFG-VS signal from the fused-quartz surface. Not only there is no time-dependent SFG-VS signal from the fused quartz surface, but also there is no SFG-VS frequency domain spectra in the 2300-2380 cm^{-1} range from this surface. In comparison, there is also no such spectra from the gold film surface or the α-quartz surface in this range, except the non-resonant IR pulse spectral profile from the cross-correlation with the ps visible pulse as shown in Figure 2E. When the IR beam path is not purged, there is a dip in the IR spectral profile with the shape of the gaseous CO_2 absorption (Figure 2E inset), and the dip disappears with the purge using the N_2 gas. With or without purge, the gold film surface, as well as the quartz and fused silica surfaces, is exposed in the ambient atmosphere. All these suggest that there is no observable adsorbed molecular monolayer on the gold film or quartz surfaces, otherwise SFG-VS spectral interference with the non-resonant substrate contribution to the SFG-VS should have been readily observed,[37, 44, 45] or SFG-VS spectra of trace impurity molecules on a surface without non-resonant background would also have appeared from that of the fused silica surface.[46] As there is no explicit possibility for the observed signal coming from the surface molecular species, it is imperative to understand the origin and the mechanism of the observed time-dependent SFG-VS signal.

The fact that the SFG-VS signal at the time 0 is more than two orders of magnitude stronger than that of the time-delayed SFG-VS signal does not suggest that the effect of the much weaker time-delayed SFG-VS signal on the overall SFG-VS spectral measurement is insignificant, particularly for the case of SFG-VS from the gold film surface. As we have known, the SFG-VS spectrum is proportional to the Fourier transform of the time-dependent SFG-VS signal.[47] For example, the SFG-VS spectra of ODT (octadecanethiol) monolayer on the gold surface appeared

as several small dips on the overall SFG-VS signal profile.[44] If it is measured in the time-domain SFG-VS as in Figure 4A, the time 0 peak is going to be significantly stronger than the time-delayed signal. To remove this strong non-resonant SFG response at time zero, time-delayed SFG-VS spectral measurement were used,[48-50] despite the fact that the spectra so-obtained will have somewhat distorted spectral lineshape due to the time-delay.[33, 47] Nevertheless, the unexpected signal in the time-dependent SFG-VS measurement observed here, and its impact to the SFG-VS spectral measurement need to be further investigated.

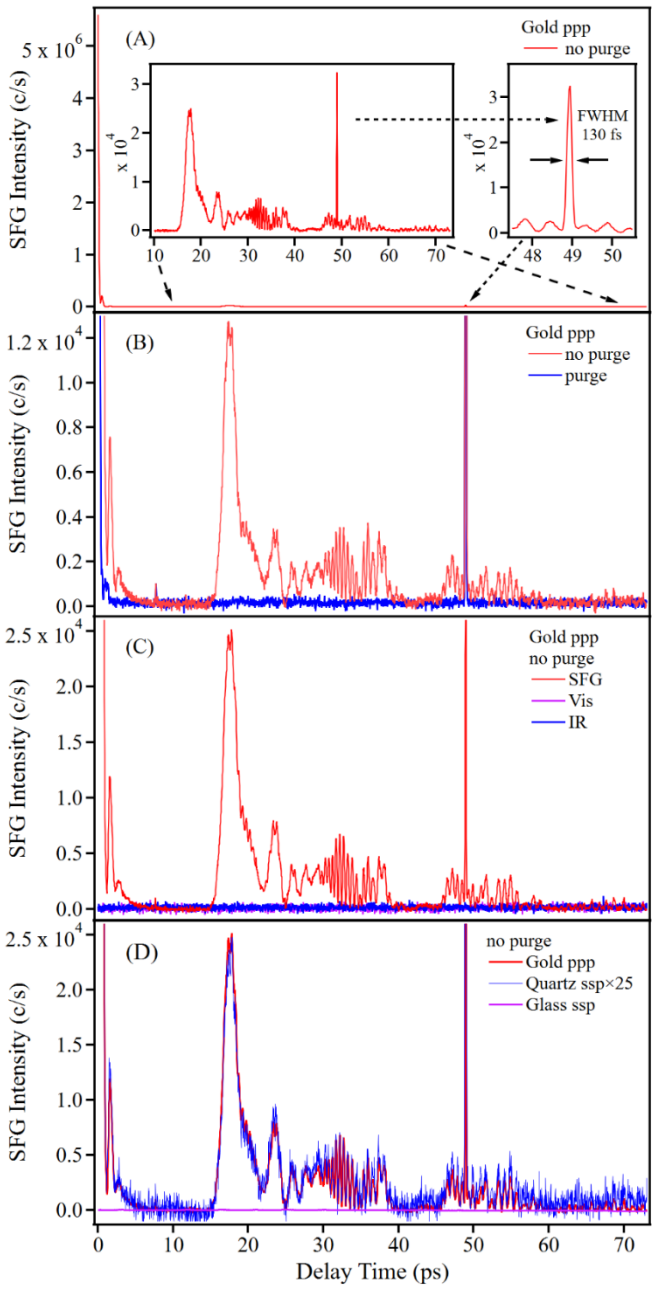

FIG.4. To understand the time dependent SFG-VS signal from the gold film surface. (A) The peak at time zero is the cross correlation of the fs visible and IR pulse (FWHM =114.5±0.7 fs). Signal with a ~ 15-70 ps delay (left inset) shows complex coherent oscillation patterns, and the sharp peak at ~ 49ps (right inset) has a width of ~140fs. (B) Time-dependent SFG-VS signal without and with the N_2 purge of the IR beam path. The ~ 15-70 ps oscillation pattern completely disappears, and the ~ 49 ps peak remains. (C) Both the oscillation pattern and the ~49 ps peak disappear when the fs visible or IR beam is blocked, indicating its SFG-VS nature. (D) The same oscillation pattern and ~ 49 ps peak remain after replacing the gold film with a thick z-cut quartz crystal, and they completely disappear with a fused silica surface.

Moreover, the SFG-VS signal from the z-cut quartz surface has been known to come from the bulk nonlinear signal of the α-quartz bulk within the coherent length of the SFG-VS processes. To confirm this picture, we tried to measure the time-dependent SFG-VS signal from a *β*-BBO crystal substrate surface (Figure 5). The time-dependent SFG-VS signal from the *β*-BBO crystal substrate surface again shows exactly the same oscillation pattern as that of the gold film surface under the same laser pulse and experimental conditions. In the meantime, the SFG-Vs signal intensity from the *β*-BBO crystal substrate surface is 1.6 x10^5 times of that of the gold film surface. This reflects the much larger second order SFG-VS susceptibility of the *β*-BBO crystal over that of the z-cut α-quartz crystal, as well as that of the gold film. This clearly provide a further improvement of the detection sensitivity of the time-dependent SFG-VS phenomenon originated from this new nonlinear process observed in this experiment.

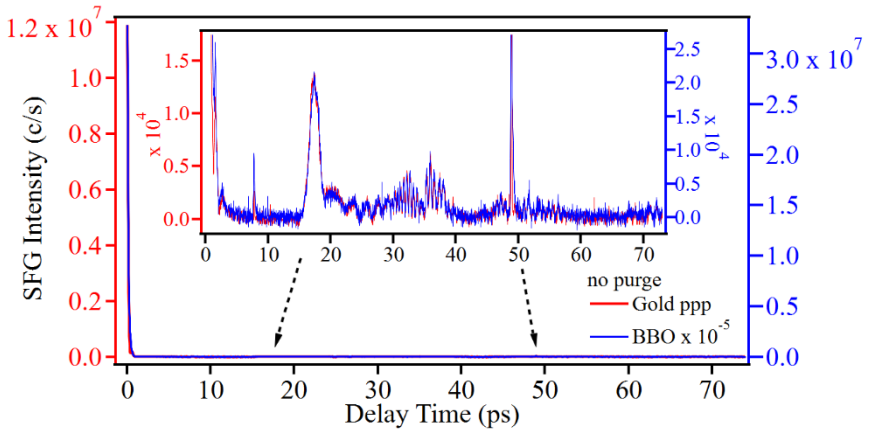

FIG. 5. Time-dependent SFG-VS spectrum from the *β*-BBO crystal substrate surface and the gold film surface in the *ppp* polarization combination. Neutral density filters with OD = 5 was used to reduce the significantly larger signal from the *β*-BBO crystal substrate surface. The ~49 ps spike remains in the *β*-BBO data, and it was attributed to a weak sideband either in the visible or IR laser pulses, as discussed in the main text.

2. Mechanism and Simulation of the Observed Time-Dependent SFG-VS Signal

From the data in the above section, one sees that a). the observed signal is the result of both the visible and IR pulses acting together, i.e., from some kind of 'sum-frequency' process; b). the observed time-dependent 'sum-frequency' signal is not from the molecular species adsorbed on the respective surfaces, but from the atmospheric gaseous CO_2 molecules in the IR beam path; c). the time-dependent 'sum-frequency' signal generated with the gold surface, α-quartz crystal surface and β-BBO crystal surface in the reflective geometry all have the same oscillation pattern but orders of magnitude different signal intensities. One cannot help surmising that such 'sum-frequency' signal is only possible from the up-conversion process of the IR emission of the atmospheric gaseous CO_2 molecules in the IR beam path by the visible pulses at those surfaces. It is, therefore, a detection of the infrared free-induction decay (IR-FID) emission of the atmospheric gaseous CO_2 molecules through an up-conversion process. This can be detected simply because that the up-conversion process on the gold film surface is just sensitive enough to enable the detection of the up-converted IR-FID signal in our conventional broadband SFG-VS and SFG-FID setup. For the case of gold film surface, it is the surface-enabled up-conversion of IR-FID process.

The absorption of the ultrafast IR pulse create a macroscopic coherent polarization, and this polarization radiates and decays immediately following the absorption and the creation of the coherent polarization in the same direction and with the same polarization, as it is called the infrared free induction decay (FID) process. Thus, this IR-FID radiation transmits in the same direction following the IR laser beam and is up-converted at the gold film surface to generate the additional time-dependent SFG-VS signal. This SFG-VS signal is actually the surface enabled up-conversion of the IR-FID process (Figure 6C-6D). In comparison, in the normal SFG-FID process (Figure 6A-6B), where the molecules are on the surface and the molecular coherence created by the ultrafast IR pulses interacts directly with the probing ultrafast visible pulse to generate the SFG-FID emission signal, there is no actual IR emission process involved; while in this surface-enabled up-conversion of IR-FID process, the molecules are not on the surface, and there is actual coherent IR emission following the absorption of the ultrafast IR light (Figure 6C-6D). The fact that the normal SFG-FID process of molecules on the surface and the IR-FID process of the

molecules in the IR beam path up-converted on the surface are both detected in the same SFG-VS setup makes it necessary to clearly distinguish them from each other and to evaluate its impact in the SFG-VS measurement. The IR-FID contribution to the SFG-VS signal can be avoided if there is no absorbing species in the IR beam path or there is no up-conversion enabling surface, such as the gold film surface in this case. For the study in this work, the IR-FID signal can be easily avoided by purging to remove the atmospheric CO_2 in the IR beam path (Figure 4B). However, the contribution from the upconverted IR-FID process is unavoidable in studying buried electrode interfaces, where a partially absorbing electrolyte layer is usually present and a gold film or other substrate with significant non-resonant SFG response is usually used as electrode.[48, 51] Moreover, the time-delayed SFG-VS spectra also include the contribution of the up-converted IR-FID process from the coherent emission of the IR absorbing layer, making the interpretation of the SFG-VS data for such systems even more complicated. The only thing one can pray is that in the specific buried interface under study, the up-converted IR-FID contribution is significantly smaller than that of the surface SFG-VS process. No matter what, a clear understanding on the surface-enabled up-conversion of the IR-FID and proper assessment of its possible contribution for such interfaces is important.

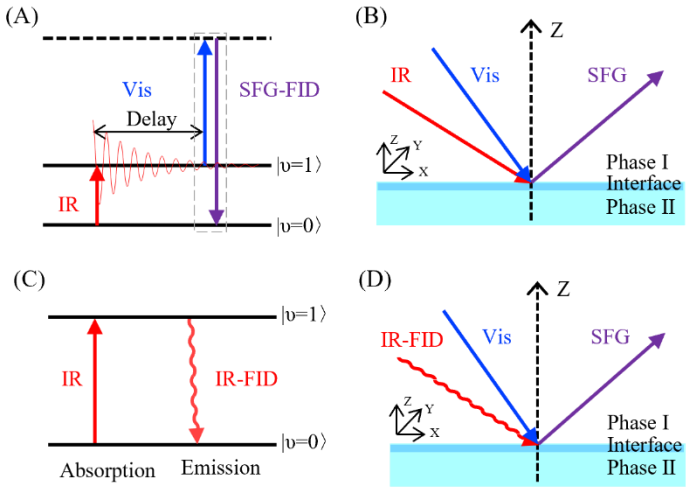

FIG. 6. Surface SFG-FID vs. surface enabled up-conversion of IR-FID. **(A-B)** In the SFG-FID, the molecules are on the surface, and the delayed visible pulse probes the vibrational coherence of the surface molecules and directly generate the SFG-FID signal. The surface molecules directly interact with both the IR and the visible pulses. **(C-D)** In surface enabled up-conversion IR-FID, the molecules in the IR beam

path are not on the surface and they generate IR-FID emission after the absorption of the IR light following the IR beam path, and the emitted IR photons are thus up-converted by mixing with the visible pulse on the surface with different time delay. Only the IR pulse interact with the molecules and the visible pulse does not.

Usually, ultrafast IR-FID from liquid or gaseous samples were detected using up-conversion process in bulk nonlinear crystals in the transmission geometry.[13] Therefore, it is not surprising that with nonlinear crystals such as α-quartz and *β*-BBO crystals, up-conversion of the IR-FID signal in the reflection geometry also works. In comparison, the phase matching condition in the reflection geometry is less favorable to generate the up-conversion signal as high as that in the transmission geometry. However, the up-conversion on the gold film surface requires essentially no additional phase-matching condition, and the up-conversion efficiency is orders of magnitude lower than that from the high-efficiency nonlinear crystals, such as *β*-BBO crystals (Figure 5). It is therefore quite unexpectable that such up-conversion process is actually detectable from the gold film surface in this report, and besides, so far there has no explicit report on such observation.

Nevertheless, if the above mechanism is correct, the oscillation patterns in the observed up-converted time-dependent IR-FID signal can also be understood from the IR-FID emission process of the atmospheric CO_2 molecules. The strong and broad atmospheric CO_2 absorption band in the range of 2300-2380 cm^{-1} (Figure 2E & Figure 7A) corresponds to the antisymmetric stretching mode of CO_2 molecule, usually called the 4.26 μm band. At room temperature, the actual absorption spectrum of the gaseous CO_2 molecules consists of many sharp ro-vibrational lines in the R (ΔJ = +1) and P (ΔJ = -1) branches (Figure 7B). J is the rotational quantum number. For linear molecules such as CO_2, the Q (ΔJ = 0) branch is forbidden. This band in the spectra in Figure 2E and Figure 7A is broad and continuous without the ro-vibrational line structure, only because the spectral resolution in obtaining the spectra is about 10 cm^{-1}. The spectral intensity of the ro-vibrational absorption lines of the gaseous CO_2 molecules at 1 atm pressure and 296K temperature with 30% humidity can be obtained from the HITRAN (High-resolution Transmission, https://hitran.org/) database (Figure 7B). [14, 52, 53] The IR-FID emission is the results of the time-dependent coherent evolution of the macroscopic polarization after the absorption of the

broadband ultrafast IR pulse. Therefore, the intensity of time-dependent IR-FID emission (I_{FID}) is proportional to the expression approximated in Equation 1. This expression is essentially the solution to the optical Bloch equation with only the linear (homogeneous) relaxation term as approximation.[47, 54, 55]

$$I_{FID} = |E_{FID}|^2 \propto \left| \sum_i \sqrt{S(i)} \cdot e^{-i2\pi\nu_i t} \cdot \sqrt{I_{IR}(\nu_i)} \cdot e^{-t/\tau_i} \right|^2 \quad (1)$$

in which i represents the ro-vibrational line used in the calculation; $S(i)$ is the spectral line intensity of the ith ro-vibrational line (Figure 7B) at the given ambient temperature and pressure conditions;[56] t is the time after absorption, i.e. the delay time; ν_i is the frequency of the ith ro-vibrational line; $I_{IR}(\nu_i)$ is the IR intensity at the frequency of the ith ro-vibrational line in the broad band ultrafast IR pulse; $\sum_i$ represents the sum over states (SOS) of all the ro-vibrational line with the IR excitation range; τ_i is the vibrational linear dephasing time of the ro-vibrational excited state i.

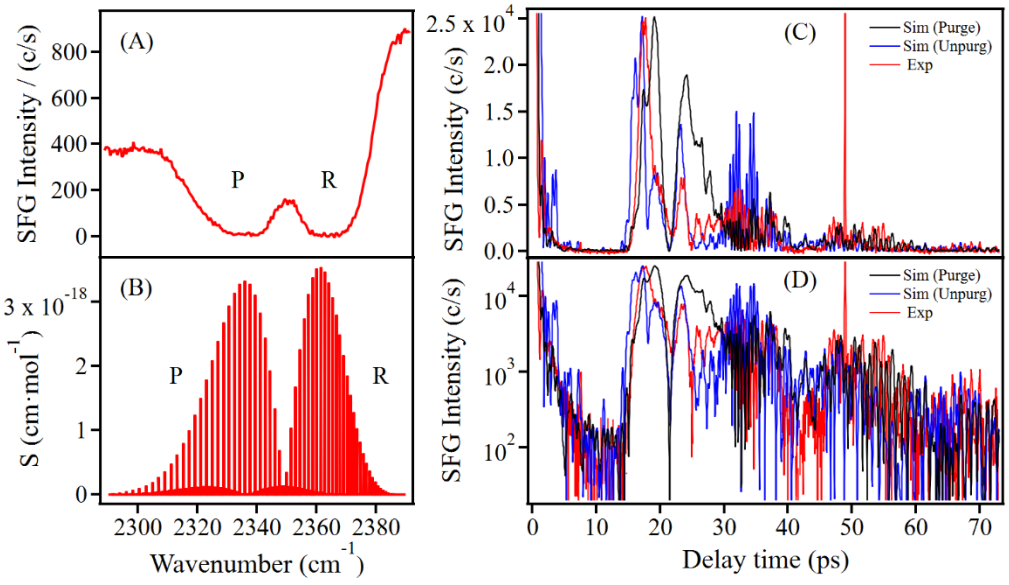

FIG.7. (A) Absorption spectra of gaseous CO_2 molecules in the IR beam path measured with the 10 cm^{-1} resolution SFG-VS on gold film surface as in Figure 2E; (B) Ro-vibrational spectral line intensity (S, in the cm per molecule unit) plot of the antisymmetric stretching band of $^{12}C^{16}O_2$ (abundance 0.98)

simulated from HITRAN at 296K, 1 atm.[56] (C) The time-dependent SFG-VS experimental data and the IR-FID simulation using the HITRAN data; (D) Data in (C) with logarithmic unit.

Figure 7C shows the experimental data and the simulation (in relative intensity scale) results of the time-dependent IR-FID trace using the ro-vibrational line data in Figure 7B with purged and unpurged (also in Figure 7A) IR profiles as shown in Figure 2E in the range of 2290-2390 cm^{-1}, with an overall relaxation time τ_i = 25 ps. Supposedly, τ_i can be different for each ro-vibrational state. However, for describing the main time-evolution features, when without prior knowledge of the dephasing time of each state, τ_i for the ro-vibrational line of the same vibration transition can roughly take the same approximate value in the simulation. Figure 7D is with the same data in Figure 7C plotted in logarithmic scale. It is important to see in these data that the main features, particularly the oscillation period and overall profile, of the simulated results resemble the IR-FID experimental measurements. Moreover, the simulated results also reproduced the signal gap of more than 10 ps between the time-zero peak and the first major emission peak. These explicitly suggest that the IR-FID of the gaseous CO_2 in the IR path after ultrafast IR excitation is indeed the most likely mechanism of the observed time-dependent signal. Similar simulation of the coherence of the ro-vibrational states of the antisymmetric stretching mode of the atmospheric CO_2 molecules was carried out for the interference pattern in the time-resolved visible spectrum generated through ultrabroadband four-wave mixing (FWM) process.[57] In comparison, the simulated pattern and the experimental interference pattern in this work resemble each other much more closely than that in this previous work. This suggests that the IR-FID mechanism as we have proposed describes the observed time-resolved data as good as it can be.

The differences between the purged and unpurged IR profiles are expected, as they give different weight of each of the terms to be summed up in the Equation 1. The actual excitation profile is most likely in between these two extreme cases of the IR intensity profiles, more or less closed to the unpurged profile judged from the differences from the data. As one can see, the gaseous CO_2 molecules in the atmosphere along the IR beam path which is about 1.6 meters long are all possible contributors to the overall measured signal in Figure 7C, making the accurate

determination their distribution in the IR path an complicated job. It would be much better to control those factors in the IR-FID measurements by purging the whole IR path, and using a gas cell with a relatively short path length, filled with air, or CO_2 gas mixtures with known partial pressures. Such experiments are underway and will be reported in the future. Nevertheless, as the time-zero in the measurement is set when the fs IR pulse and the fs visible pulse overlap simultaneously on the gold surface, no matter where the CO_2 molecule in the IR path absorb and emit the IR photon, the travel distance of the IR light is always the same. Therefore, it is always the time-delay between the absorption and emission of the CO_2 molecules, which is always the same for all the CO_2 molecules in the IR optical path, that is measured by the time-delay of the fs visible pulse against the fs IR pulse.

One important fact here is that Eqn.1 only includes the IR-FID emission from the absorption of the gaseous molecules in the IR optical path, as detected through the up-conversion by the visible pulse on the gold surface, and it does not include the zero-time non-resonant SFG signal directly generated from the gold surface. Therefore, in comparison to the experimental data, the signal at the time-zero should include both the up-converted zero-time IR-FID contribution and the non-resonant direct SFG signal at the time-zero within the cross-correlation time between the femtosecond IR and visible pulses, whose FWHM is about 115 fs. In the simulation, the relative strength of these two contributions are not known *a prior*. Therefore, we do not include it in the simulation here. The relative strength as well as relative phase of these two contributions at the time-zero needs further investigation in the future. Nevertheless, there is a zero-time coherence in the IR-FID radiation as shown in the simulation results, and it also warrants future investigation. Eqn.1 also neglects the convolution with the time profiles of the femtosecond IR and visible laser pulses. Because the cross correlation of the IR and visible pulse is with a FWHM about 115 fs, such convolution will not result significant changes to the time-dependent oscillation patterns spanned over several tens of picoseconds, except for slight broadening of each of the much narrower oscillation peaks, which are usually with ~250 fs FWHM.

The IR-FID intensity with β-BBO crystal (Figure 5) has signal intensity five orders more than that from the gold surface. This suggests that the IR-FID signal can be detected with the same sensitivity by using β-BBO crystal from the CO_2 molecules in the same air sample with more than five orders of magnitude shorter path length, i.e. a 16 μm in comparison to the 1.6 m path length with the measurement on the gold surface. Considering the fact that the typical CO_2 content in air is about 0.04% by volume, i.e., about 400 ppm, sub-ppb level detection of the CO_2 molecule in gas samples with the long path length, or with multiple IR reflection cell, is also possible, opening the IR-FID measurement possible to interesting applications.

3. IR-FID of atmospheric H_2O

Water (H_2O) vapor is Earth's most abundant greenhouse gas. Water molecule in the atmosphere also absorbs and emits infrared photons as the atmospheric CO_2. We expect that similar IR-FID signal should be observed in our time-dependent SFG measurement on the gold surface by tuning the fs IR pulse wavelength to the water absorption bands in the 3400 – 4000 cm^{-1}. In our lab condition with about 40% humidity, the content of water is about 1% in volume, about 25 time of that of CO_2.

The data and simulation of the IR-FID measurement of the atmospheric H_2O are shown in Figure 8. Figure 8A shows the unpurged IR profile measured on the gold surface with the 10 cm^{-1} resolution ps visible pulse. Figure 8B shows the ro-vibrational spectral line intensity at ambient condition from HITRAN. Figure 8C-8D are the time-resolved IR-FID data and simulation using the data from the profiles in Figure 8A and Figure 8B and the Equation 1 with an uniform τ_i = 18 ps, in normal and logarithmic scale, respectively.

Water is a non-linear molecule, unlike the linear CO_2. Therefore, at room temperature, the P-, Q-, and R- branches of the ro-vibrational spectrum are all present and their frequencies are all mixed-up. Unlike the regularly-separated ro-vibrational spectral lines for the atmospheric CO_2 molecules (Figure 7B), the spectral lines for the atmospheric H_2O molecules appear to be more randomly spread over the frequency range (Figure 8B). As the result, the interference pattern in Figure 8C from the coherent IR-FID emissions of the atmospheric H_2O molecules is more

complicated than the interference pattern from that of the CO_2 molecules (Figure 4A). Particularly, for the CO_2 case, there is a signal gap of more than 10 ps between the time-zero peak and the first major emission peak beginning around 14 ps (Figure 4A). There is no such gap for the H_2O time-dependent data (Figure 8C). There is also no apparent oscillation pattern with regular period for the H_2O time-dependent IR-FID data as that for CO_2. Nevertheless, the simulated time-dependent interference patterns for the H_2O and the CO_2 molecules explicitly captured the main features in their experimental data, respectively. This is a confirmation of the IR-FID mechanism as proposed above.

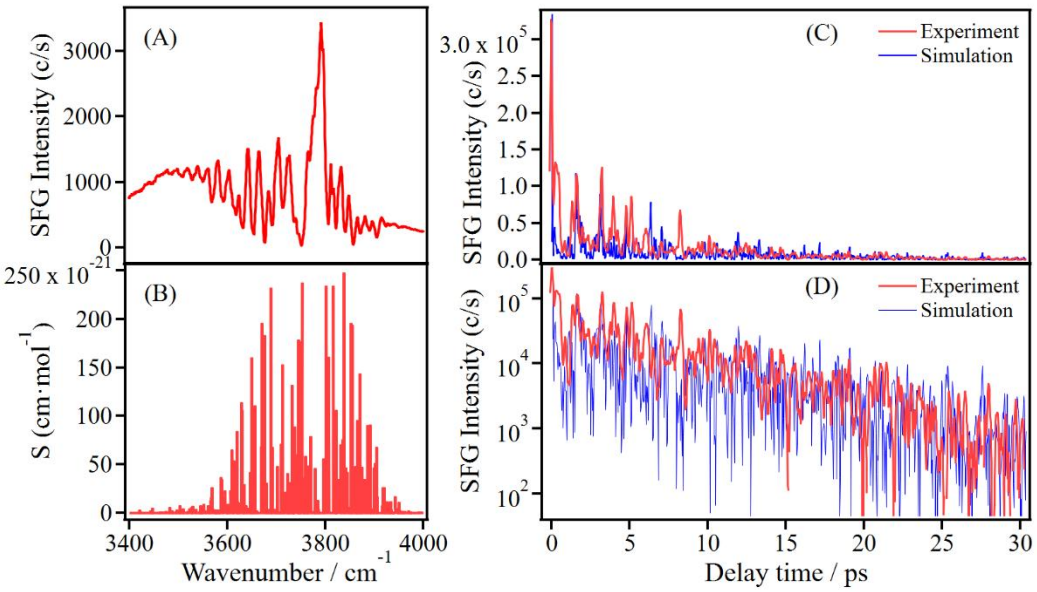

FIG.8. (A) Absorption spectra of gaseous H_2O molecules in the IR beam path measured with the 10 cm^{-1} resolution SFG-VS on gold film surface; (B) Ro-vibrational spectral line intensity (S, in the cm per molecule unit) plot of the antisymmetric stretching band of $H_2{}^{16}O$ (abundance 0.99) simulated from HITRAN at 296K, 1 atm.[56] (C) The time-dependent SFG-VS experimental data and the IR-FID simulation using the HITRAN data; (D) Data in (C) with logarithmic unit.

4. IR-FID of a 10 μm Polyethylene Film

Solid material in the fs IR optical path can also absorb and emit IR light like the gaseous atmospheric CO_2 and H_2O molecules. Its time-dependent IR-FID emission after absorption of the fs IR light can also be up-converted by the fs visible pulse on gold surface, or using quartz or β-

BBO crystal. Spectroscopically, the main difference between the molecules in solid or liquid and the gaseous molecules is that there is no rotational lines for the absorption spectra of the former. Nevertheless, the IR-FID radiation from the solid or liquid molecules still remains with much shorter coherence time[13] than that of the gaseous molecules, e.g. the CO_2 molecules.

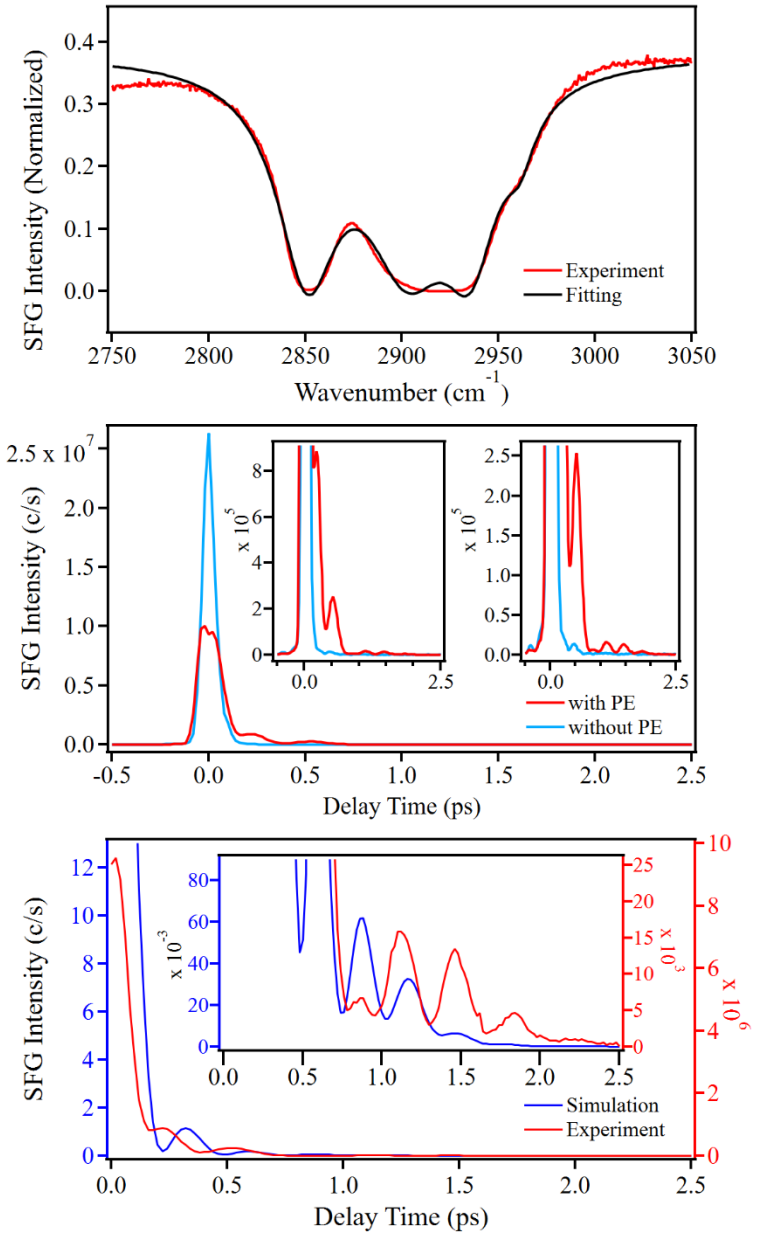

FIG. 9. (A) Absorption spectra and its fitting of a 10 μm thick polyethylene (PE) film in the IR beam path measured with the 10 cm^{-1} resolution SFG-VS on gold film surface (normalized over the SFG-VS spectra from gold film surface without inserting PE film). Fitting parameters: A_1 = - 5.9 ± 0.2, ν_1 = 2850.8 ± 0.2

cm^{-1}, Γ_1 = 18.9 ± 0.4 cm^{-1}; A_2 = - 8.1 ± 0.6, ν_2 = 2902.8 ± 0.7 cm^{-1}, Γ_2 = 27.5 ± 1.3 cm^{-1}; A_3 = - 4.2 ± 0.5, ν_3 = 2935.6 ± 0.4 cm^{-1}, Γ_3 = 17.4 ± 1.2 cm^{-1}; A_4 = - 0.7 ± 0.1; ν_4 = 2961.2 ± 0.6 cm^{-1}, Γ_4 = 9.4 ± 1.2 cm^{-1}. (B) The time-dependent SFG-VS spectra with and without insertion of the PE film in the infrared light path. (C) The time-dependent SFG-VS experimental data and the IR-FID simulation.

Here, Figure 9B shows the time-dependent signal from a 10 μm thick polyethylene film using broadband fs IR light centered at 2900 cm^{-1} (with FWHM = 380 cm^{-1}), which covers the entire C-H stretching absorptions of polyethylene in the range of 2800-3000 cm^{-1}. Without the PE film inserted into the femtosecond IR beam path, there is no time-dependent signal after the time-zero peak, which is the result of the non-resonant SFG-VS signal from the gold surface (Figure 9B). However, after inserting the PE film, this time-zero peak is reduced due to the absorption of the IR light by the PE film (Figure 9A), and several peaks with about 300 fs interval appears in the following 2.5 ps time delay range (Figure 9B), consistent with the short coherence time for the IR-FID from molecules in solid and liquid. The oscillation pattern is the result of the beatings between the various IR vibrational modes coherently excited by the broadband femtosecond IR light.[33] Figure 9C shows the comparison of the experimental data with the IR-FID simulation using the eqn. 1, using the fitting parameters of the peak positions (ν_i), widths (FWHM = $2\Gamma_i = 1/\pi c\tau_i$) and relative amplitudes (A_i for $S(i)$) of the four apparent absorption peaks in Figure 9A, with $\sqrt{I_{IR}(\nu_i)}$ = 1, i.e. the simplest IR profile. In fitting the IR absorption spectra (Figure 9A), the Lorentzian lineshape formula for the intensity $I = I_0 + \sum_i \frac{A_i \Gamma_i}{(\nu - \nu_i)^2 + \Gamma_i^2}$ is used. Even though the fittings of the absorption curve (Figure 9A) is less ideal, due to the fact that the absorption of the strongest absorption peak is already saturated for the 10 mm thick PE film, and the Lorentzian lineshape is only an approximation, the simulated curve reproduces the oscillation periods of the experimental data rather well (Figure 9C). One can notice that the simulated oscillation pattern decays faster than that in the experimental data. This is likely due to the fact that the Lorentzian lineshape approximation used to obtain the spectral parameters in the simulation assumes the whole width of each peak is due to the coherent decay of the vibration, which over-estimated the

coherent decay rate and resulted in faster coherent decay in the simulation results. In addition, to make a better quantitative comparison, PE film with less thickness need to be used to avoid the saturated absorption in the IR bands (Figure 9A). However. PE film with thickness thinner than 10 μm is not commercially available or can be customer-made. Nevertheless, from the data and simulation in Figure 9, the IR-FID mechanism for the time-dependent SFG-VS signal emerged from the IR absorption by the PE film in the IR optical path can be concluded.

There was a recent report about the effects on the SFG-VS spectrum from the gold film surface with and without inserting a 10 μm thickness PE film in the IR beam path.[35] In this report, the focus was on the emergence of additional peaks in a series of SFG-VS spectra (with spectral resolution about 7 cm^{-1}) from bare gold film surface with 500 fs delay steps up to 2.5 ps. These spectra peaks were interpreted as '*abnormal spectral bands in BB-SFG induced by bulk absorption and refraction*'. There was another recent report discussing the thickness dependence on those '*abnormal spectral bands*' using PDMS (polydimethylsiloxane) films with thickness from 5.5 to 14.5 μm.[36] These studies are contingent to the SFG-VS measurement on buried interfaces, as any IR absorbing medium in the IR path before the IR beam arriving the surface can cause '*abnormal*' spectral peaks, i.e. making it not '*bulk-free*', in the SFG-VS measurement.[35, 36] Understanding the mechanism of such phenomenon, and proper normalization schemes need to be carefully implemented to eliminate such '*abnormal*' bands in the SFG-VS measurement.

As we have shown in Figure 3, '*abnormal*' bands from the gaseous CO_2 molecules can appear in the SFG-VS spectral measurement at different delays. As we can understood now, they are the results of the upconverted IR-FID radiations from the CO_2 molecules after absorption of the femtosecond IR light. The same up-converted IR-FID radiation can result in SFG-VS measurements in the form of total time-dependent signal measured with fs visible pulse in the time-domain (Figure 4), or in the form of time-dependent spectra with ps visible pulse in the frequency-domain (Figure 3).[47] The '*abnormal*' bands in the case of the PE and PDMS films can also be understood with the same IR-FID up-conversion mechanism, and can be treated both in the time-domain and frequency-domain in a unified way. We also showed above that the time-

dependent SFG-VS signal after PE absorption from the gold film surface can be understood with the IR-FID up-conversion mechanism. It frequency-domain spectra were also obtained, in agreement with the time-domain data. These data are not discussed in detail here, as they are consistent with the data previous literature works and they were discussed intensively there as the so-called '*abnormal*' bands.[35]

In SFG-VS experiment, the '*abnormal*' bands due to the up-conversion process of the IR-FID radiation in the SFG-Vs measurement can only present when the SFG-VS measurement is carried out on a surface, such as the gold film surface, or on a nonlinear optical substrate, such as the α-quartz crystal or β-BBO crystals, as they both have the capability to generate enough up-conversion signal from the IR-FID radiation. For such cases, particularly for the metal electrode surface SFG-VS studies, the '*abnormal*' bands due to the up-converted IR-FID radiation will appear in the measured SFG-VS signal, making the interpretation of the SFG-VS data more complicated. Such issue has to be explicitly investigated in any future studies. As we have understood, the contribution to the overall SFG-VS signal by the up-converted IR-FID radiation due to the bulk molecular absorption cannot be simply removed with the time-delayed techniques aimed to remove the non-resonant background centered at the time-zero,[30, 48] special attention needs to be taken to deal with those '*abnormal*' bands from the absorbing bulk in the interpretation of the SFG-VS spectrum of such buried interfaces.[35, 36]

On the other hand, such '*abnormal*' bands in SFG-VS spectra will not be measurable in SFG-VS for the non-upconverting substrate surface, such as the fused silica, glass, or CaF_2 surface, even when they are the buried interface. The absorbing layer in the IR beam path before such non-upconverting buried interface simply absorbs and modulates the IR intensity at the interface, and can be corrected accordingly, for obtaining the SFG-VS spectra of the interface.

IV. CONCLUSIONS

In our SFG-VS experiment on the gold film surface, we accidentally observed frequency and time-dependent SFG-VS spectra in the infrared frequency region of the CO_2 antisymmetric

stretching vibrational modes. Follow-up experiments trying to understand the origin and mechanism of these unexpected SFG-VS spectra led us to find that the gold film surface acts to up-convert the coherent IR-FID radiation from the gaseous CO_2 molecules in the femtosecond IR beam path with the visible pulse into our surface SFG-VS signal. We also showed that the IR-FID radiation from the atmospheric H_2O molecules and a thin solid PE film can also be detected through the up-conversion on the gold film surface. These results in the contributions to the SFG-VS signal with non-interfacial origin.

The appearance of the SFG-VS signal with non-interfacial origin poses serious problem in SFG-VS as an interfacial-selective spectroscopic probe.[58, 59] Luckily, such up-conversion process of the IR-FID can only happen on surfaces with significantly larger second-order optical response, such as the gold film surface, or on non-linear optical crystal surface or bulk, such as the α-quartz and β-BBO crystals. The fact that gold film surface can up-convert the IR-FID radiation into the SFG-VS signal complicates the SFG-VS study of the electrochemical surfaces, where gold film surface is usually used, covered with electrolyte solutions which can absorb the IR light and the radiate IR photons. Even with a few micrometer thickness, the electrolyte solution can significantly absorb the IR light and result in coherent IR-FID radiation. In such a way, 'abnormal spectral bands' can be observed in the SFG-VS measurement on gold film surfaces.[35, 36] Such 'abnormal spectral bands' now can be understood with mechanism of the up-converted IR-FID radiation. This understanding of the IR-FID up-conversion mechanism in contributing to the SFG-VS signal can help such SFG-VS studies on electrochemical interface, as well as other interfaces where such IR-FID contribution to the SFG-VS signal may occur. Methods to explicitly distinguish or quantitatively remove the possible IR-FID contribution from the true surface contribution to the observed SFG-VS signal in electrochemical interfaces and other studies need to be developed.

In addition, it has been known that the time and frequency resolved measurement of the coherent IR-FID radiation from the molecules in the gas phase and condensed phases can be sensitively measured through up-conversion using nonlinear crystals. The β-BBO results in this study indicates that ppb level concentration of gaseous CO_2 and H_2O molecules is detectable. As

IR-FID radiation contains information of the ultrafast coherent molecular vibrational dynamics and the interactions that can affect such dynamics, one may find applications using IR-FID in atmospheric and combustion studies. Molecular vibration is particularly sensitive to local environment and interactions. Sensitive measurement of coherent IR-FID radiation can also provide an approach for applications for chemical and dynamical processes in complex liquids and in biological systems. Further exploration in such direction is warranted

AUTHOR INFORMATION

Corresponding Author

*(H.-F. Wang) E-mail: wanghongfei@westlake.edu.cn

First Author

(B. J. Zhao) E-mail: zhaobojun@westlake.edu.cn

Other Authors

(X.-X. Peng) E-mail: pengxingxing@westlake.edu.cn

(L. Zhang) E-mail: zhangli@westlake.edu.cn

(J. M. Cao) E-mail: caojingming@westlake.edu.cn

(S.-Y. Yang) E-mail: yangshuyi@westlake.edu.cn

(A.-A. Liu) E-mail: liuaa@baqis.ac.cn

ORCID

Bo-Jun Zhao: 0000-0002-2926-4371

Xing-Xing Peng: 0000-0003-1468-2770

Li Zhang: 0000-0002-2905-8260

Jing-Ming Cao: 0009-0007-6395-5516

Shu-Yi Yang: 0009-0000-9138-4609

An-An Liu: 0009-0001-8191-6111

Hong-Fei Wang: 0000-0001-8238-1641

Notes

The authors declare no competing financial interest.

ACKNOWLEDGMENTS

B.J.Z. thanks Wanghua Hu in Xiao Lin's group at Westlake University for coating gold film on the K9 glass. This work was supported by the National Natural Science Foundation of China (NSFC Grant No. 21727802) and Westlake Education Foundation.

References

(1) Bloch, F. Nuclear Induction. *Physical Review* **1946**, *70* (7-8), 460-474. DOI: 10.1103/PhysRev.70.460.

(2) Hahn, E. L. Nuclear Induction Due to Free Larmor Precession. *Physical Review* **1950**, *77* (2), 297-298. DOI: 10.1103/PhysRev.77.297.2.

(3) Brewer, R. G.; Shoemaker, R. L. Optical Free Induction Decay. *Physical Review A* **1972**, *6* (6), 2001-2007. DOI: 10.1103/PhysRevA.6.2001.

(4) Hopf, F. A.; Shea, R. F.; Scully, M. O. Theory of Optical Free-Induction Decay and Two-Photon Superradiance. *Physical Review A* **1973**, *7* (6), 2105-2110. DOI: 10.1103/PhysRevA.7.2105.

(5) Zewail, A. H.; Orlowski, T. E.; Dawson, D. R. Incoherent resonance decay and coherent optical ringing from coherently prepared electronic states: a new technique for probing phase memory and radiationless relaxation in gases and solids. *Chemical Physics Letters* **1976**, *44* (2), 379-384. DOI: https://doi.org/10.1016/0009-2614(76)80535-0.

(6) Zewail, A. H.; Godar, D. E.; Jones, K. E.; Orlowski, T. E.; Shah, R. R.; Nichols, A. Coherent Optical Spectroscopy Of Molecules And Molecular Beams. Vol. 0113; SPIE, 1977; pp 42-56.

(7) Jones, K. E.; Nichols, A.; Zewail, A. H. High-resolution time resolved spectroscopy of collisionless molecular beams. II. Energy randomization and optical phase relaxation of molecules in crossed laser and molecular beams. *The Journal of Chemical Physics* **2008**, *69* (7), 3350-3362. DOI: 10.1063/1.436989.

(8) Orlowski, T. E.; Jones, K. E.; Zewail, A. H. Measurements of molecular dephasing and radiationless decay by laser-acoustic diffraction spectroscopy. *Chemical Physics Letters* **1978**, *54* (2), 197-202. DOI: https://doi.org/10.1016/0009-2614(78)80082-7.

(9) Orlowski, T. E.; Zewail, A. H. Radiationless relaxation and optical dephasing of molecules excited by wide- and narrow-band lasers. II. Pentacene in low-temperature mixed crystals. *The Journal of Chemical Physics* **2008**, *70* (3), 1390-1426. DOI: 10.1063/1.437579.

(10) de Vries, H.; Wiersma, D. A. Fluorescence transient and optical free induction decay spectroscopy of pentacene in mixed crystals at 2 K. Determination of intersystem crossing and internal conversion rates. *The Journal of Chemical Physics* **2008**, *70* (12), 5807-5822. DOI: 10.1063/1.437411.

(11) Stoutland, P. O.; Dyer, R. B.; Woodruff, W. H. Ultrafast Infrared Spectroscopy. *Science* **1992**, *257* (5078), 1913-

1917.
(12) Beckerle, J. D.; Cavanagh, R. R.; Casassa, M. P.; Heilweil, E. J.; Stephenson, J. C. Subpicosecond transient infrared spectroscopy of adsorbates. Vibrational dynamics of CO/Pt(111). *The Journal of Chemical Physics* **1991**, *95* (7), 5403-5418. DOI: 10.1063/1.461657.
(13) Crowell, R. A.; Holtom, G. R.; Xie, X. S. Infrared Free Induction Decay of Liquid Water Molecules. *The Journal of Physical Chemistry* **1995**, *99* (7), 1840-1842. DOI: 10.1021/j100007a009.
(14) Hammond, T. J.; Monchocé, S.; Zhang, C.; Brown, G. G.; Corkum, P. B.; Villeneuve, D. M. Femtosecond time-domain observation of atmospheric absorption in the near-infrared spectrum. *Physical Review A* **2016**, *94* (6), 063410. DOI: 10.1103/PhysRevA.94.063410.
(15) Coddington, I.; Swann, W. C.; Newbury, N. R. Time-domain spectroscopy of molecular free-induction decay in the infrared. *Opt. Lett.* **2010**, *35* (9), 1395-1397. DOI: 10.1364/OL.35.001395.
(16) Chesnokov, E. N.; Kubarev, V. V.; Koshlyakov, P. V.; Kulipanov, G. N. Direct observation of the terahertz optical free induction decay of molecular rotation absorption lines in the sub-nanosecond time scale. *Applied Physics Letters* **2012**, *101* (13). DOI: 10.1063/1.4754826.
(17) Shen, Y. R. Surface properties probed by second-harmonic and sum-frequency generation. *Nature* **1989**, *337* (6207), 519-525. DOI: 10.1038/337519a0.
(18) Eisenthal, K. B. Liquid interfaces probed by second-harmonic and sum-frequency spectroscopy. *Chem. Rev.* **1996**, *96* (4), 1343-1360, Review. DOI: 10.1021/cr9502211.
(19) Wang, H. F.; Velarde, L.; Gan, W.; Fu, L. Quantitative sum-frequency generation vibrational spectroscopy of molecular surfaces and interfaces: lineshape, polarization, and orientation. *Annu Rev Phys Chem* **2015**, *66*, 189-216. DOI: 10.1146/annurev-physchem-040214-121322.
(20) Miranda, P. B.; Shen, Y. R. Liquid Interfaces: A Study by Sum-Frequency Vibrational Spectroscopy. *The Journal of Physical Chemistry B* **1999**, *103* (17), 3292-3307. DOI: 10.1021/jp9843757.
(21) Somorjai, G. A.; Rupprechter, G. Molecular studies of catalytic reactions on crystal surfaces at high pressures and high temperatures by infrared-visible sum frequency generation (SFG) surface vibrational spectroscopy. *J. Phys. Chem. B* **1999**, *103* (10), 1623-1638, Review. DOI: 10.1021/jp983721h.
(22) Nihonyanagi, S.; Mondal, J. A.; Yamaguchi, S.; Tahara, T. Structure and Dynamics of Interfacial Water Studied by Heterodyne-Detected Vibrational Sum-Frequency Generation. In *ANNUAL REVIEW OF PHYSICAL CHEMISTRY, VOL 64*, Johnson, M. A., Martinez, T. J. Eds.; Vol. 64; 2013; pp 579-603.
(23) Guyot-Sionnest, P. Coherent processes at surfaces: Free-induction decay and photon echo of the Si-H stretching vibration for H/Si(111). *Phys Rev Lett* **1991**, *66* (11), 1489-1492. DOI: 10.1103/PhysRevLett.66.1489.
(24) Owrutsky, J. C.; Culver, J. P.; Li, M.; Kim, Y. R.; Sarisky, M. J.; Yeganeh, M. S.; Yodh, A. G.; Hochstrasser, R. M. Femtosecond coherent transient infrared spectroscopy of CO on Cu(111). *The Journal of Chemical Physics* **1992**, *97* (6), 4421-4427. DOI: 10.1063/1.463884.
(25) Star, D.; Kikteva, T.; Leach, G. W. Surface vibrational coherence at the CaF2/air interface: Vibrational wave packet dynamics as a probe of interface inhomogeneity. *The Journal of Chemical Physics* **1999**, *111* (1), 14-17. DOI: 10.1063/1.479251.
(26) Roke, S.; Kleyn, A. W.; Bonn, M. Time- vs. frequency-domain femtosecond surface sum frequency generation. *Chemical Physics Letters* **2003**, *370* (1), 227-232. DOI: https://doi.org/10.1016/S0009-2614(03)00085-X.
(27) Bordenyuk, A. N.; Benderskii, A. V. Spectrally- and time-resolved vibrational surface spectroscopy: ultrafast hydrogen-bonding dynamics at D2O/CaF2 interface. *J Chem Phys* **2005**, *122* (13), 134713. DOI: 10.1063/1.1873652.

(28) Bordenyuk, A. N.; Jayathilake, H.; Benderskii, A. V. Coherent Vibrational Quantum Beats as a Probe of Langmuir−Blodgett Monolayers. *The Journal of Physical Chemistry B* **2005**, *109* (33), 15941-15949. DOI: 10.1021/jp051632g.
(29) Stiopkin, I. V.; Jayathilake, H. D.; Weeraman, C.; Benderskii, A. V. Temporal effects on spectroscopic line shapes, resolution, and sensitivity of the broad-band sum frequency generation. *The Journal of Chemical Physics* **2010**, *132* (23). DOI: 10.1063/1.3432776.
(30) Curtis, A. D.; Asplund, M. C.; Patterson, J. E. Use of Variable Time-Delay Sum-Frequency Generation for Improved Spectroscopic Analysis. *The Journal of Physical Chemistry C* **2011**, *115* (39), 19303-19310. DOI: 10.1021/jp2069368.
(31) Shalhout, F. Y.; Malyk, S.; Benderskii, A. V. Relative Phase Change of Nearby Resonances in Temporally Delayed Sum Frequency Spectra. *The Journal of Physical Chemistry Letters* **2012**, *3* (23), 3493-3497. DOI: 10.1021/jz3014437.
(32) Velarde, L.; Wang, H.-f. Capturing inhomogeneous broadening of the –CN stretch vibration in a Langmuir monolayer with high-resolution spectra and ultrafast vibrational dynamics in sum-frequency generation vibrational spectroscopy (SFG-VS). *The Journal of Chemical Physics* **2013**, *139* (8). DOI: 10.1063/1.4818996.
(33) Velarde, L.; Lu, Z.; Wang, H. f. Coherent Vibrational Dynamics and High-resolution Nonlinear Spectroscopy: A Comparison with the Air/DMSO Liquid Interface. *Chinese Journal of Chemical Physics* **2013**, *26* (6), 710-720. DOI: 10.1063/1674-0068/26/06/710-720.
(34) Boulesbaa, A.; Borguet, E. Vibrational Dynamics of Interfacial Water by Free Induction Decay Sum Frequency Generation (FID-SFG) at the Al2O3(1120)/H2O Interface. *J Phys Chem Lett* **2014**, *5* (3), 528-533. DOI: 10.1021/jz401961j.
(35) He, Y.; Zhang, Y.; Ren, H.; Wang, J.; Guo, W.; Sun, S.-G.; Wang, Z. Abnormal spectral bands in broadband sum frequency generation induced by bulk absorption and refraction. *Opt. Express* **2019**, *27* (20), 28564-28574. DOI: 10.1364/OE.27.028564.
(36) Liu, X.; Guo, W.; He, Y.; Huangfu, Z.; Yu, W.; Ning, Q.; Wang, Z. Thickness-dependent IR distortion from bulk absorption and refraction and its effects on broadband sum frequency generation spectroscopy. *Applied Physics Express* **2021**, *14* (11), 112001. DOI: 10.35848/1882-0786/ac2a58.
(37) Hu, X.-H.; Wei, F.; Wang, H.; Wang, H.-F. α-Quartz Crystal as Absolute Intensity and Phase Standard in Sum-Frequency Generation Vibrational Spectroscopy. *The Journal of Physical Chemistry C* **2019**, *123* (24), 15071-15086. DOI: 10.1021/acs.jpcc.9b03202.
(38) Ma, G.; Liu, J.; Fu, L.; Yan, E. C. Y. Probing Water and Biomolecules at the Air–Water Interface with a Broad Bandwidth Vibrational Sum Frequency Generation Spectrometer from 3800 to 900 cm−1. *Appl. Spectrosc.* **2009**, *63* (5), 528-537.
(39) Rao, Y.; Comstock, M. J.; Eisenthal, K. B. Absolute orientation of molecules at interfaces. *The journal of physical chemistry. B* **2006**, *110 4*, 1727-1732. DOI: 10.1021/jp055340r.
(40) Esenturk, O.; Walker, R. A. Surface vibrational structure at alkane liquid/vapor interfaces. *J Chem Phys* **2006**, *125* (17), 174701. DOI: 10.1063/1.2356858.
(41) Jones, A. C.; Kunz, M. B.; Tigges-Green, I.; Zanni, M. T. Dual spectral phase and diffraction angle compensation of a broadband AOM 4-f pulse-shaper for ultrafast spectroscopy. *Opt Express* **2019**, *27* (26), 37236-37247. DOI: 10.1364/OE.27.037236.
(42) Sussman, B. J.; Lausten, R.; Stolow, A. Focusing of light following a 4-fpulse shaper: Considerations for quantum control. *Physical Review A* **2008**, *77* (4). DOI: 10.1103/PhysRevA.77.043416.

(43) Nihonyanagi, S.; Eftekhari-Bafrooei, A.; Borguet, E. Ultrafast vibrational dynamics and spectroscopy of a siloxane self-assembled monolayer. *J Chem Phys* **2011**, *134* (8), 084701. DOI: 10.1063/1.3518457.
(44) Richter, L. J.; Petralli-Mallow, T. P.; Stephenson, J. C. Vibrationally resolved sum-frequency generation with broad-bandwidth infrared pulses. *Opt. Lett.* **1998**, *23* (20), 1594-1596. DOI: 10.1364/ol.23.001594.
(45) Fu, L.; Chen, S. L.; Wang, H. F. Validation of Spectra and Phase in Sub-1 cm(-1) Resolution Sum-Frequency Generation Vibrational Spectroscopy through Internal Heterodyne Phase-Resolved Measurement. *J Phys Chem B* **2016**, *120* (8), 1579-1589. DOI: 10.1021/acs.jpcb.5b07780.
(46) Bian, H. T.; Feng, R. R.; Xu, Y. Y.; Guo, Y.; Wang, H. F. Increased interfacial thickness of the NaF, NaCl and NaBr salt aqueous solutions probed with non-resonant surface second harmonic generation (SHG). *Phys. Chem. Chem. Phys.* **2008**, *10* (32), 4920-4931, Review. DOI: 10.1039/b806362a.
(47) Velarde, L.; Wang, H. F. Unified treatment and measurement of the spectral resolution and temporal effects in frequency-resolved sum-frequency generation vibrational spectroscopy (SFG-VS). *Phys Chem Chem Phys* **2013**, *15* (46), 19970-19984. DOI: 10.1039/c3cp52577e.
(48) Lagutchev, A.; Hambir, S. A.; Dlott, D. D. Nonresonant background suppression in broadband vibrational sum-frequency generation spectroscopy. *J. Phys. Chem. C* **2007**, *111* (37), 13645-13647, Letter. DOI: 10.1021/jp075391j.
(49) Carter, J. A.; Wang, Z. H.; Dlott, D. D. Ultrafast Nonlinear Coherent Vibrational Sum-Frequency Spectroscopy Methods To Study Thermal Conductance of Molecules at Interfaces. *Accounts Chem. Res.* **2009**, *42* (9), 1343-1351, Review. DOI: 10.1021/ar9000197.
(50) Quast, A. D.; Curtis, A. D.; Horn, B. A.; Goates, S. R.; Patterson, J. E. Role of Nonresonant Sum-Frequency Generation in the Investigation of Model Liquid Chromatography Systems. *Anal. Chem.* **2012**, *84* (4), 1862-1870, Article. DOI: 10.1021/ac2032035.
(51) Nicolau, B. G.; García-Rey, N.; Dryzhakov, B.; Dlott, D. D. Interfacial Processes of a Model Lithium Ion Battery Anode Observed, in Situ, with Vibrational Sum-Frequency Generation Spectroscopy. *The Journal of Physical Chemistry C* **2015**, *119* (19), 10227-10233. DOI: 10.1021/acs.jpcc.5b01290.
(52) Gordon, I. E.; Rothman, L. S.; Hargreaves, R. J.; Hashemi, R.; Karlovets, E. V.; Skinner, F. M.; Conway, E. K.; Hill, C.; Kochanov, R. V.; Tan, Y.; et al. The HITRAN2020 molecular spectroscopic database. *Journal of Quantitative Spectroscopy and Radiative Transfer* **2022**, *277*, 107949. DOI: https://doi.org/10.1016/j.jqsrt.2021.107949.
(53) Rothman, L. S.; Hawkins, R. L.; Wattson, R. B.; Gamache, R. R. Energy levels, intensities, and linewidths of atmospheric carbon dioxide bands. *Journal of Quantitative Spectroscopy and Radiative Transfer* **1992**, *48* (5), 537-566. DOI: https://doi.org/10.1016/0022-4073(92)90119-O.
(54) Mukamel, S. *Principles of nonlinear optical spectroscopy*; Oxford University Press Oxford, 1999.
(55) Hamm, P.; Zanni, M. T. *Concepts and methods of 2D infrared spectroscopy*; Cambridge University Press Cambridge, 2011.
(56) *HITRANonline-Line-by-Line Search*. https://hitran.org/lbl/.
(57) Lanin, A. A.; Voronin, A. A.; Fedotov, A. B.; Zheltikov, A. M. Time-domain spectroscopy in the mid-infrared. *Sci Rep* **2014**, *4*, 6670. DOI: 10.1038/srep06670.
(58) Shen, Y. R. Bask Theory of Surface Sum-Frequency Generation. *J. Phys. Chem. C* **2012**, *116* (29), 15505-15509, Article. DOI: 10.1021/jp305539v.
(59) Wang, H.-F. Sum frequency generation vibrational spectroscopy (SFG-VS) for complex molecular surfaces and interfaces: Spectral lineshape measurement and analysis plus some controversial issues. *Progress in Surface Science* **2016**, *91* (4), 155-182. DOI: https://doi.org/10.1016/j.progsurf.2016.10.001.